The Cryosphere Discuss., 9, 6423–6470, 2015
www.the-cryosphere-discuss.net/9/6423/2015/
doi:10.5194/tcd-9-6423-2015

The Cryosphere Discussions
Open Access
EGU

Modeling debris-covered glaciers: extension due to steady debris input

L. S. Anderson[1] **and R. S. Anderson**[2]

[1]Institute of Earth Sciences, University of Iceland, Askja, Sturlugötu 7, 101 Reykjavìk, Iceland
[2]Institute of Arctic and Alpine Research, and Department of Geological Sciences, University of Colorado, Campus Box 450, Boulder, Colorado 80309, USA

Received: 30 September 2015 – Accepted: 13 October 2015 – Published: 23 November 2015

Correspondence to: L. S. Anderson (leif@hi.is)

Published by Copernicus Publications on behalf of the European Geosciences Union.

Abstract

Debris-covered glaciers are common in rapidly-eroding alpine landscapes. When thicker than a few centimeters, surface debris suppresses melt rates. If continuous debris cover is present, mass balance gradients can be reduced leading to increases in glacier length. In order to quantify feedbacks in the debris-glacier-climate system, we developed a 2-D long-valley numerical glacier model that includes englacial and supraglacial advection. We ran 120 simulations in which a steady state debris-free glacier responds to a step increase of surface debris deposition. Simulated glaciers advance to steady states in which ice accumulation equals ice ablation, and debris input equals debris loss from the glacier. Our model and parameter selections produce two-fold increases in glacier length. Debris flux onto the glacier and the relationship between debris thickness and melt rate strongly control glacier length. Debris deposited near the equilibrium-line altitude, where ice discharge is high, results in the greatest glacier extension when other debris related variables are held constant. Continuous debris cover reduces ice discharge gradients, ice thickness gradients, and velocity gradients relative to initial debris-free glaciers. Debris-forced glacier extension decreases the ratio of accumulation zone to total glacier area (AAR). The model reproduces first-order relationships between debris cover, AARs, and glacier surface velocities from glaciers in High Asia. We provide a quantitative, theoretical foundation to interpret the effect of debris cover on the moraine record, and to assess the effects of climate change on debris-covered glaciers.

1 Introduction

Glaciers erode landscapes directly by subglacial quarrying and abrasion, and indirectly by steepening hillslopes above glaciers. Oversteepened hillslopes can deliver loose rock (debris) onto glacier surfaces (Benn and Evans, 2010). Steep hillslopes and high hillslope erosion rates in alpine settings therefore tend to correspond with the

TCD
9, 6423–6470, 2015

occurrence of debris-covered glaciers (e.g., the Himalaya and the Alaska Range; Scherler et al., 2011b). We refer to a debris-covered glacier as any glacier with continuous debris cover across the full glacier width over a portion of the glacier (after Kirkbride, 2011).

Debris cover more than a few centimeters thick damps the melt rate of underlying ice (e.g., Østrem, 1959; Shroder et al., 2000; Owen et al., 2003). If debris supply is high to a glacier surface, mass balance profiles can be greatly altered, leading to increases in glacier volume and length (e.g., Scherler et al., 2011b; Fig. 1). Thick debris cover on glaciers can also lead to low accumulation-area ratios (AARs; Scherler et al., 2011b). Paleoclimate estimates will be exaggerated if typical AARs are assumed when reconstructing past climate from former debris-covered glacial moraines.

Debris-covered glaciers exhibit a wide range of responses to climate change (Scherler et al., 2011a). While Himalayan debris-free glaciers are almost coherently retreating, Himalayan debris-covered glaciers are not responding coherently to climate change. Some Himalayan debris-covered glaciers are advancing, others are stationary, and yet others are retreating (e.g., Raper and Braithwaite, 2006; Scherler et al., 2011a; Benn et al., 2012; Banerjee and Shankar, 2013). However, there is a strong trend toward negative mass balance for most of these debris-covered glaciers (Bolch et al., 2011; Benn et al., 2012).

In situ documentation of debris-covered glacier mass loss is made difficult by non-uniform debris thicknesses and the presence of scattered ice cliffs and surface ponds. As a result, in situ debris thickness, sub-debris melt rates, sub-debris ice thickness measurements and complete summer balances are sparse (WGMS, 2008). Measurements of englacial debris concentrations and distribution are yet more difficult to obtain, but vital for predicting debris-covered glacier response to climate change (e.g., Kirkbride and Deline, 2013). In addition, exploration of century-scale response of debris-covered glaciers to climate is limited by short satellite and observational periods (Bolch et al., 2011). Logistical realities therefore limit our ability to constrain

TCD
9, 6423–6470, 2015

feedbacks between debris deposition rates, the englacial environment, the supraglacial environment, ice dynamics, and climate change.

While logistics limit our ability to directly observe some feedbacks, many of the most provocative conclusions relating debris and glacier response are based on remotely-sensed data. Scherler et al., (2011b) provided an extensive inventory of remotely-sensed velocity and debris coverage data from 287 glaciers in High Asia. They inferred that (1) hillslope debris flux onto glaciers correlates with the percentage of debris cover on glaciers; (2) debris-covered glacier AARs tend to be smaller than debris-free glaciers; and (3) surface debris perturbs velocity distributions on valley glaciers by shifting maximum glacier velocities up glacier, away from the terminus. These inferences highlight the effect of thick debris cover on valley glaciers and also act as targets for debris-covered glacier models.

Numerical models can help quantify feedbacks within the climate-debris-glacier system (e.g., Konrad and Humphrey, 2000). Debris-covered glacier models have been used to explore the response of valley glaciers to (1) the constant input of debris (Konrad and Humphrey, 2000); (2) one-time landslide deposition of debris on glaciers (Vacco et al., 2010; Menounos et al., 2013); and (3) climate change (Naito et al., 2000; Banerjee and Shankar, 2013). Konrad and Humphrey (2000) used a two-dimensional (2-D; long-valley-vertical) model with a constant surface slope to explore debris-covered glacier dynamics. In their model, debris was deposited on the glacier surface below the equilibrium line altitude (ELA) and then advected along the glacier surface. With high debris fluxes, simulated glaciers formed several-meter thick debris covers, which reduced sub-debris melt toward zero, and resulted in glaciers that never reached steady state. Numerical models have shown that large landslides onto glaciers can lead to multiple-kilometer advances of the terminus (Vacco et al., 2010; Menuounos et al., 2013). Debris-covered glacier retreat response timescales have also been explored with a simplified debris-covered glacier model (Banerjee and Shankar, 2013). However, because of the complexity of the debris-glacier-climate system, many feedbacks remain unexplored.

TCD
9, 6423–6470, 2015

In this study, we isolate the effect of debris on valley glaciers independent of climate change. Debris fluxes, deposition rates, deposition zone widths, and deposition locations vary from glacier to glacier (Fig. 1), yet we know little about how changes in these debris related variables effect glaciers. So we ask: What about debris delivery controls glacier response?

In many debris-covered glacier systems, debris is deposited in the accumulation zone, advected through the glacier following englacial flowpaths, and emerges in the ablation zone (e.g., Boulton and Eyles, 1979; Owen and Derbyshire, 1989; Benn and Owen, 2002; Benn et al., 2012). In order to explore the response of glaciers to surface debris cover, we formulated a new transient 2-D numerical model (x, z) that couples debris deposition, englacial debris advection, debris emergence, surface debris advection, debris-melt coupling, and shallow-ice-approximation dynamics (Figs. 1 and 2). By coupling these components, we are able to explore the sensitivity of debris-covered glaciers to changes in debris input related variables (across the entire glacier) and compare our theory-based results with Scherler et al. (2011b)'s dataset. To isolate the effect of debris, we start each simulation with a steady state debris-free (ssdf) glacier and impose a step change increase in debris deposition rate. This study lays the foundation for future modeling efforts exploring the response of debris-covered glaciers to climate change.

2 Theory and numerical methods

We employ a 2-D finite difference numerical model (in downvalley and vertical, x and z) that can simulate the evolution of temperate valley glacier response to climate and debris. Forced by a time series of equilibrium-line altitudes (ELAs) and a prescribed mass balance gradient, the model calculates ice surface elevations above a longitudinal profile by solving equations for ice flux and mass conservation. The modeled longitudinal path represents the glacier centerline. A number of authors have used the shallow-ice-approximation (SIA) and basal sliding parameterizations in

TCD
9, 6423–6470, 2015

numerical glacier models (e.g., Nye 1965; Budd and Jensen, 1975; Oerlemans, 1986; MacGregor et al., 2000; Kessler et al., 2006). We employ a similar approach, but add a longitudinal stress coupling parameterization (Marshall et al., 2005). The model is efficient, allowing wide exploration of parameter space in simulations over thousands of years.

2.1 Conservation of ice mass

Mass conservation is at the core of the ice physics model. Assuming uniform ice density, and ignoring variations in the width of the glacier, conservation of ice requires that

$$\frac{\partial H}{\partial t} = \dot{b} - \frac{\partial Q}{\partial x}, \tag{1}$$

where x is the distance along the glacier flowline, H is the local ice thickness, $\dot{b}$ is the local specific balance, and Q is the specific volume discharge of ice $[=] \mathrm{m}^3\,\mathrm{m}^{-1}\,\mathrm{yr}^{-1}$. This requires a prescribed mass balance field, and a prescription of the ice physics governing ice discharge.

2.2 Annual surface mass balance of ice in the absence of debris

We use a simple mass balance scheme that limits the number of parameters while honoring the essence of glacier surface mass balance. We combine surface accumulation and ablation into a single thresholded net mass balance profile as a function of elevation, z:

$$\dot{b}_z = \min\left(\frac{\mathrm{d}\dot{b}_z}{\mathrm{d}z}(Z_{\mathrm{ice}} - \mathrm{ELA}), \dot{b}_z^{\max}\right), \tag{2}$$

TCD
9, 6423–6470, 2015

where $\frac{d\dot{b}_z}{dz}$ is the mass balance gradient with elevation, Z_{ice} is the ice surface elevation and $\dot{b}_z^{max}$ is a maximum mass balance that accounts for the depletion of moisture available for precipitation at higher elevations.

2.3 Annual surface mass balance: effect of supraglacial debris

Sub-debris melt rate decreases in an exponential or hyperbolic fashion with increasing debris thickness (e.g., Østrem, 1959; Nicholson and Benn, 2006). For debris layers thinner than a critical thickness (~ 2 cm), surface debris can increase melt rates relative to bare ice. For debris thicknesses greater than ~ 2 cm, debris suppresses sub-debris melt rates relative to bare ice (e.g., Nicholson and Benn, 2006; Fig. 3). We assume that heat is transferred through the debris layer by conduction. Sub-debris melt should therefore vary inversely with debris thickness (i.e., be hyperbolic) and change based on the temperature gradient $\sim (T_s - T_{ice})/h_{debris}$ (e.g., Nicholson and Benn, 2006). Here, $T_{ice} = 0$. We neglect the melt-amplifying effects of very thin debris for simplicity and represent the damping of sub-debris melt rates with

$$b' = \dot{b}_z \left(\frac{h_*}{h_* + h_{debris}} \right), \tag{3}$$

where h_* is a characteristic length scale

$$h_* = \frac{k\overline{T}_s}{(1-\phi)\rho_i L f_{pdd} \overline{T}_a} \tag{4}$$

and k and ϕ are thermal conductivity and porosity of debris cover, ρ_i and L the density and latent heat of fusion of ice, $\overline{T}_s$ the average debris surface temperature, $\overline{T}_a$ the average screen-level air temperature, and f_{pdd} is a positive degree day factor relating air temperature and the bare ice melt rate (e.g. Mihalcea et al., 2006). In this formulation, sub-debris melt rates approach bare-ice melt rates as debris thins ($h_{debris} \ll h_*$), and

TCD
9, 6423–6470, 2015

asymptote towards zero melt as debris thickens ($h_{debris} \gg h_*$). We use h_* values based on data from 15 studies (Fig. 3; $h_* = 0.066 \pm 0.029$ m (1σ), and ranges from 0.03 to 0.13 m). We also show the most likely exponential fit to the data for comparison to the most likely hyperbolic fit (Fig. 3). The exponential curve fit declines toward zero melt more rapidly than the hyperbolic fit. We neglect the effects of surface streams, thermokarst, and ice cliffs that can lead to complex local topography and melt rates within debris covers (e.g., Reid and Brock, 2014; Anderson, 2014).

2.4 Ice dynamics

Ice is transferred down valley by internal ice deformation and by basal motion. The ice discharge down glacier is:

$$Q = H\overline{u} \tag{5}$$

in which H is the local ice thickness and $\overline{u}$ is the depth-averaged bed parallel velocity that results from the sum of the ice deformation velocity and basal motion. The SIA reduces the momentum balance equations to expressions for vertical shear stress as a function of the local ice surface slope and ice thickness. The depth-averaged horizontal velocity due to internal deformation is

$$\overline{u}_{def} = \frac{2A}{n+2}(\rho_i g \alpha)^{n-1} H^n \tau_{bx}, \tag{6}$$

where ρ_i the density of ice, g the acceleration due to gravity, α the local ice surface slope, H the local ice thickness, τ_{bx} is the local basal shear stress, A is the creep parameter, and n is the flow law exponent (assumed to be 3). We assume that all ice is temperate, and A is therefore taken to be 24×10^{-25} [$Pa^{-3} s^{-1}$] (Cuffey and Paterson, 2010). In addition to internal deformation, temperate glaciers transfer mass via basal slip due to ice sliding over the bed and deformation of the bed itself. We assume that all basal slip is accomplished by sliding over bedrock, and follow the formulation of Kessler

TCD
9, 6423–6470, 2015

et al. (2006):

$$u_{\text{sliding}} = u_c e^{1-\frac{\tau_c}{\tau_{bx}}} \tag{7}$$

where u_c is a typical sliding velocity, and τ_c is the gravitational driving stress that gives rise to the typical sliding velocity. This sliding parameterization is not as sensitive to high τ_b values as many other sliding laws, and provides a more conservative estimate of sliding velocities when $\tau_b > \tau_c$ (Kessler et al., 2006). We have modified the *SIA* equations by including a parameterization of longitudinal stress coupling (after Marshall et al., 2005) and a shapefactor, f, that represents the effect of valley wall drag. The longitudinal coupling scheme modifies τ_{bx} to

$$\tau_{bx} = f\left(\rho_i g H \alpha + 4\overline{\eta} H \frac{\partial^2 u}{\partial x^2} + 4\frac{\partial \overline{\eta} H}{\partial x}\frac{\partial u}{\partial x}\right), \tag{8}$$

where the effective viscosity, $\overline{\eta} = \frac{1}{2}[A\tau_E^{n-1}]^{-1}$. In the shallow ice approximation, τ_E, the effective stress, is approximated by the local τ_{bx} (after Cuffey and Paterson, 2010). We take $f = 0.75$ to approximate the effects of sidewall drag from a parabolic valley cross-section with a half-width 3 times the ice thickness (Cuffey and Paterson, 2010).

2.5 Ice velocity structure within the glacier

Horizontal and vertical velocity fields must be resolved within the glacier in order to advect englacial debris. We start by defining the horizontal velocity field within the glacier, and then employ continuity in an incompressible medium to calculate the associated vertical velocities. The $u(z)$ profile shape may be obtained from the analytic solution to flow of ice in a uniform channel with Glen's flow law rheology:

$$F = 5\left(\left(\zeta - 1.5\zeta^2\right) + \zeta^3 - \frac{1}{4}\zeta^4\right), \tag{9}$$

TCD
9, 6423–6470, 2015

where ζ is the non-dimensional height z/H above the bed, and $F = \frac{u(z)}{\overline{u}_{\text{def}}}$ is the ratio of horizontal speed to mean deformation speed. The full horizontal velocity field is then characterized by

$$U_\zeta(x,\zeta) = \overline{u}_{\text{def}}(x)F + u_{\text{sliding}}(x) + u_{\text{coupling}}(x), \tag{10}$$

where u_{coupling} is the vertically-integrated velocity effect due to longitudinal stress coupling.

Vertical and horizontal velocity fields ($w(x,z)$ and $u(x,z)$) are related through the continuity equation for an incompressible fluid, which in two dimensions (x,z) is:

$$\frac{\partial w}{\partial z} = -\frac{\partial u}{\partial x}. \tag{11}$$

We then solve for the vertical velocity in each cell within each column by integrating vertically:

$$w = -\int_0^z \left(\frac{\partial u}{\partial x}\right) \mathrm{d}z, \tag{12}$$

employing the boundary condition that $w = 0$ at $z = 0$ (i.e., we assume no basal melt). Vertical velocities, w, at the glacier surface must be equal in magnitude and opposite in sign to the surface mass balance field, and are therefore directed downward at the ice surface in the accumulation zone, and upward in the ablation zone.

2.6 Debris deposition

Debris can be entrained in the glacier at either the upper glacier surface or at the glacier bed. Supraglacial debris deposition largely occurs by mass wasting from hillslopes above glaciers, while sub-glacial debris entrainment occurs through regelation and

TCD
9, 6423–6470, 2015

net freeze-on. Basal debris emergence at the glacier surface is typically limited to the glacier toe and likely plays a minor role in the formation of extensive debris covers (Benn and Evans, 2010). We focus on debris sourced from valley head and side walls. Headwall erosion rates are better constrained than subglacial entrainment rates and mass wasting from head and sidewalls is the primary process of debris delivery onto many valley glaciers (Messerli and Zurbuchen, 1968; Humlum, 2000 (European Alps); Owens and Derbyshire, 1989 (Karakoram); Ballantyne and Harris, 1994; Humlum, 2000 (West Greenland); Benn and Owen, 2002 (Himalaya); Humlum, 2005 (Svalbard); Arsenault and Meigs, 2005 (Southern Alaska); O'Farrell et al., 2009 (Southern Alaska); Benn and Evans, 2010; Scherler et al., 2011b (High Asia)). The model replicates the deposition of debris onto the glacier surface leading to the formation of Ablation-dominant and Avalanche-type medial moraines on the glacier surface (Benn and Evans, 2010). For simplicity, we neglect englacial thrusting and ice-stream interaction moraines (medial moraines associated with tributary junctions; see Eyles and Rogerson, 1978; Anderson, 2000; Benn and Evans, 2010). These cases can be treated in subsequent modeling that incorporates the 2-D planform complexities of valley glaciers.

Debris delivery to glacier surfaces can vary considerably from glacier to glacier, depending on glacier topology and above-glacier topography (e.g., Deline, 2009). We capture this complexity using four variables: the total debris flux to the glacier surface ($d_{\mathrm{flux}}\,[=]\,\mathrm{m}^3\,\mathrm{m}^{-1}\,\mathrm{yr}^{-1}$), the debris deposition rate ($\dot{d}$), the debris deposition zone width ($\dot{d}_{\mathrm{width}}$), and the debris deposition location ($\dot{d}_{\mathrm{loc}}$). In the model, d_{flux} is representative of the integrated effects of $\dot{d}$ and $\dot{d}_{\mathrm{width}}$.

Rock type, slope, and fracture density are significant factors determining hillslope erosion rates and therefore also control the debris deposition rate, $\dot{d}$ (e.g., Stock and Montgomery, 1999; Molnar et al., 2007). In the model, $\dot{d}$, is allowed to vary from 1 to $8\,\mathrm{mm\,yr}^{-1}$ and is steady within each simulation (Fig. 1b). Debris deposition rate

TCD
9, 6423–6470, 2015

depends on a number of site-specific variables:

$$\dot{d} = f_{\text{funneling}} f_{\text{hillslope}} \dot{\epsilon} \frac{H_{\text{wall}}}{\tan(\theta)\mathrm{d}x}, \tag{13}$$

where $f_{\text{funneling}}$ is a dimensionless factor capturing the effect of topographic funneling on debris deposition, $f_{\text{hillslope}}$ is the percentage of the headwall that is exposed bedrock, $\dot{\epsilon}$ is the hillslope backwearing rate in $\mathrm{m\,yr^{-1}}$, H_{wall} is the height of the headwall, and θ is the headwall slope. The deposition rates explored in this study are viable deposition/hillslope erosion rates for high-relief mountain environments (e.g., Heimsath and McGlynn, 2008; Ouimet et al., 2009; Ward and Anderson, 2011). $\dot{d}_{\text{width}}$ defines the width of the deposition zone, the zone over which the debris is spread on the glacier surface (we employ a base width of 400 m; Table 1; Fig. 1b).

Debris is deposited on glaciers at locations where hillslope erosion processes are connected to the glacier surface. This requires high-relief topography above the glacier to provide the energy necessary to move the debris onto the glacier. In the model, we control the debris deposition location with the variable $\dot{d}_{\text{loc}}$, which we allow to vary from near the headwall to near the glacier terminus. $\dot{d}_{\text{loc}}$ defines the up-glacier end of the debris deposition zone.

2.7 Incorporation and advection of englacial debris

Debris deposited in the ablation zone is advected along the glacier surface, whereas debris deposited in the accumulation zone moves downward with the ice and is therefore incorporated into the glacier. Near-surface debris concentration in the accumulation zone is defined as $C_0 = \frac{\dot{d}\rho_{\text{rock}} m_z \mathrm{d}t}{H}$, where m_z is the number of vertical slices the englacial advection scheme is divided into (H/m_z being the thickness of the slices) and dt is the model time interval.

Once embedded in the glacier, C, the concentration of englacial debris $[=]\,\mathrm{kg\,m^{-3}}$, will change only by straining of the ice. Taking an Eulerian point of view, the time rate

TCD
9, 6423–6470, 2015

of change of concentration of debris within a parcel of ice is:

$$\frac{\partial C}{\partial t} = -\frac{C}{h_\zeta}\frac{\partial h_\zeta}{\partial t} - \frac{uC}{h_\zeta}\frac{\partial h_\zeta}{\partial x} - \frac{\partial (wC)}{\partial z} - \frac{\partial (uC)}{\partial x}, \tag{14}$$

where h_ζ is the cell height in a given ice column ($h_\zeta = \frac{H}{m_z}$). The first term on the right hand side represents the rate of change of C due to vertical strain of ice. Note that if the strain rate is negative, signifying vertical thinning of an ice column, debris concentration in the ice will increase. The second term represents the rate of change of C due to the longitudinal changes in glacier thickness. The third and fourth terms represent changes in C due to advection in the vertical and the horizontal directions, respectively.

2.8 Advection of debris on the glacier surface and steady states

We track both the melt-out of englacial debris and the advection of supraglacial debris on the glacier surface. The rate of change of debris thickness on the glacier surface is captured by

$$\frac{\mathrm{d}h_{\mathrm{debris}}}{\mathrm{d}t} = -\frac{Cb'}{(1-\phi)\rho_{\mathrm{rock}}} - \frac{\partial u_{\mathrm{surf}} h_{\mathrm{debris}}}{\partial x}, \tag{15}$$

where h_{debris} is the debris thickness, $\rho_{\mathrm{rock}}$is the density of the rock, ϕ is the porosity of supraglacial debris, and u_{surf} is the surface velocity of the glacier (after Konrad and Humphrey, 2000; Naito et al., 2000; Vacco et al., 2010). The first term on the right represents the addition of debris to the surface from melt of debris-laden ice. The second term represents the advection of debris down glacier.

Debris is transported off glacier by the wasting of debris down the terminal slope or by the backwasting of terminal ice cliffs (Konrad and Humphrey, 2000). The change of surface debris thickness with time at the glacier toe is:

$$\frac{\mathrm{d}h^{\mathrm{snout}}_{\mathrm{debris}}}{\mathrm{d}t} = -\frac{\mathrm{d}^{\mathrm{snout}}_{\mathrm{flux}}}{\mathrm{d}x} - \frac{Cb'}{(1-\phi)\rho_{\mathrm{rock}}} - \frac{\partial u_{\mathrm{surf}} h_{\mathrm{debris}}}{\partial x}, \tag{16}$$

TCD
9, 6423–6470, 2015

where $d_{\text{flux}}^{\text{snout}}$ is the debris flux into the foreland from the toe [=] $\text{m}^3\,\text{m}^{-1}\,\text{yr}^{-1}$. We use $d_{\text{flux}}^{\text{snout}} = \dot{b}_z^{\text{snout}} h_{\text{debris}}^{\text{snout}}$. Varying this parameterization has a minor effect on glacier length, but can have a considerable effect on the temporal evolution of the glacier as d_{flux} must equal $d_{\text{flux}}^{\text{snout}}$ for a simulated glacier to reach steady state (Appendix A). We explore the choice and effect of this parameterization in Appendix B.

3 Implementation and numerics

We now outline the order of calculations in the model. First, $\dot{b}_z$ and b' are calculated based upon elevation and debris thickness. Next, we use a second-order Runge–Kutta centered difference scheme to evolve $H(x,t)$, followed by the implementation of the debris advection schemes. We also impose a two-step anti-diffusion correction algorithm to the advection scheme (Smolarkiewicz, 1983). We test advection scheme stability using the Courant–Friedrichs–Lewy (CFL) condition, which ensures that mass is not advected beyond adjacent cells in a single timestep. We implement a terminus wedge parameterization that allows simulated glaciers to advance to steady state (Appendix A). The time step, dt, for ice-physics and debris advection is 0.01 years. All ice columns are segmented into m_z heights (i.e., $\zeta = 0 : (1/m_z) : 1$); in all results below we use $m_z = 20$ (Fig. 1b).

We select the base model parameters to represent the ablation zones of debris-covered glaciers in the Khumbu region of Nepal (Kayastha et al., 2000; Bolch et al., 2011; Benn et al., 2012; Shea et al., 2015). Base simulations run on a linear glacier bed with a basal slope of 8 % and a maximum bed elevation of 5200 m (Scherler, 2014). We use a $\frac{\text{d}\dot{b}}{\text{d}z} = 0.0075\,\text{yr}^{-1}$, which is capped at $2\,\text{m}\,\text{yr}^{-1}$ based on data from debris-free glaciers in the Khumbu region (Mera and Pokalde glaciers: after Wagnon et al., 2013). All simulations start with an 8.7 km long steady state debris-free (ssdf) glacier with a steady ELA at 5000 m ($L_{\text{ssdf}} = 8.7$ km). In each simulation a step change increase in debris deposition rate is imposed at $t = 100$ years. The base parameter set uses

TCD
9, 6423–6470, 2015

$d_{flux} = 3.2\,m^3\,m^{-1}\,yr^{-1}$, $\dot{d} = 8\,mm\,yr^{-1}$, $\dot{d}_{width}$ of 400 m, $\dot{d}_{loc}$ is 42 % from the headwall to the steady state length of the glacier, L_{ssdf}.

4 Numerical experiments and results

We first demonstrate the transfer of debris between model components and demonstrate steady state. We then explore the differences between the ssdf glacier and debris-covered glaciers and explore relative importance of $\dot{d}$, $\dot{d}_{width}$, $\dot{d}_{loc}$, and d_{flux} on glacier length. We then test the sensitivity of the model to changes in h_* and ϕ. Last, we compare our results to data from real debris-covered glaciers in High Asia.

4.1 Demonstration of debris-covered glacier steady state and conservation of debris

In order to compare steady state glacier lengths between simulations with different d_{flux} we track debris through the model. At any time in the simulation, the total debris mass that has been deposited on the simulated glacier must equal the total debris mass in the model:

$$M_{input} = M_{englacial} + M_{surface} + M_{foreland}, \quad (17)$$

where M_{input} is the total rock mass deposited on the glacier, $M_{englacial}$ is the total englacial debris mass, $M_{surface}$ is the total debris mass on the glacier surface, and $M_{foreland}$ is the total mass deposited in the proglacial environment.

We use the base parameter set simulation to highlight the transfer of debris mass through the system (Fig. 4). Because debris is deposited in the accumulation zone near the ELA, in the base simulation, $M_{englacial}$ rapidly reaches steady state (Fig. 4). As the glacier extends, $M_{surface}$ continues to increase at a declining rate as more surface debris is transferred into the foreland. The glacier reaches steady state when the glacier length, $M_{surface}$, and $M_{englacial}$ are steady and the rate of change of $M_{foreland}$ is equal the

TCD
9, 6423–6470, 2015

rate of debris input to the glacier. Each model simulation presented conserves greater than 99 % of debris mass.

4.2 Comparison of modeled debris-free and debris-covered glaciers with a steady climate

We first highlight differences in length, Q, H, and u_{surf} between the ssdf glacier and single simulated steady state debris-covered glacier (using the base parameter set; Fig. 4). In this baseline case the steady state debris-perturbed glacier length is 175 % of L_{ssdf} (Fig. 5).

h_{debris} increases down glacier from the point of initial debris emergence, $\dot{e}_{x_{int}}$, except near the glacier toe where the d^{snout}_{flux} parameterization reduces h_{debris} (Fig. 5–6). Down glacier from $\dot{e}_{x_{int}}$, gradients of Q, H, and u_{surf} are reduced relative to the debris-free glacier (Fig. 6b and d). Debris-free patterns of Q and u_{surf} are convex up near the glacier terminus, while Q and u_{surf} from debris-covered termini are concave upward. The lowest gradients in Q, H, and u_{surf} occur near the glacier terminus where h_{debris} is thickest (excluding the terminal slope; Fig. 6).

4.2.1 Comparison of debris-covered glaciers with different debris input locations

Debris input location ($\dot{d}_{loc}$) controls the englacial debris path. Debris deposited near the headwall is advected more deeply into the glacier than debris deposited near the ELA. Debris deposited near the ELA follows a shallow, short englacial path (Fig. 5). The original width of the debris band deposited in the accumulation zone, is reduced down glacier and then widens again near the surface in the ablation zone (Fig. 5). The debris band initially narrows due to the longitudinal straining of ice (Hooke and Hudleston, 1978; Cuffey and Paterson, 2010; Fig. 5a) and then widens due to feedbacks between the surface debris and ice dynamics.

TCD
9, 6423–6470, 2015

In order to highlight the effects of $\dot{d}_{loc}$ on glacier length, Q, H, and u_{surf}, we highlight three simulations where $d_{flux} = 3.2\,m^3\,m^{-1}\,yr^{-1}$, $\dot{d} = 8\,mm\,yr^{-1}$, and $\dot{d}_{width} = 400\,m$ are held constant between runs and $\dot{d}_{loc}$ is varied. $\dot{d}_{loc}$ is varied from near the top of the glacier (7 % from the headwall to L_{ssdf}; Figs. 5a and 6a and c), to near the ELA (42 % from the headwall to L_{ssdf}; Figs. 4, 5b, 6b and d), and near the debris-free glacier toe (98 % from the headwall to L_{ssdf}; Figs. 5c and 6c and e).

When debris is deposited or emerges where Q is large (near the ELA), glacier extension is greater than when debris is deposited/emerges where Q is small (near the headwall or the debris-free glacier terminus). Another way of stating this: where Q_{free}/Q_{max} nears 1 glacier extension will be largest for a given glacier (Q_{free} refers to ice discharge from the ssdf glacier and Q_{max} is the maximum Q_{free} before debris is added to the glacier). Where Q_{free}/Q_{max} nears 0 glacier extension will be small.

We ran an additional 33 simulations (36 total) in which we vary d_{flux} and $\dot{d}_{loc}$ (Fig. 7). Changes in d_{flux} are accomplished by changing $\dot{d}$ with $\dot{d}_{width}$ held constant. The importance of $\dot{d}_{loc}$ on glacier length increases with larger d_{flux} (Fig. 7). The pattern seen in Fig. 7 is insensitive to changes in the linear bed slope. Debris emergence/deposition at smaller Q leads to larger max(h_{debris}). Increasing d_{flux} leads to increases in max(h_{debris}) and the percentage of the glacier covered with debris (Fig. 8).

4.2.2 Sensitivity of steady state glacier length to changes in debris deposition rate and debris deposition zone width

Increasing either $\dot{d}$ or $\dot{d}_{width}$ leads to increases in d_{flux}, but their relative importance in governing glacier response is unclear. Does debris delivered to a small portion of a glacier at a high rate lead to a different length response than debris delivered to a glacier in a wide section but at a low rate? In order to parse the effects of $\dot{d}$ and $\dot{d}_{width}$ on glacier length, we ran 36 simulations in which we vary $\dot{d}$, $\dot{d}_{width}$, and $\dot{d}_{loc}$. Steady state glacier length increases with $\dot{d}_{width}$ when $\dot{d}_{loc}$ and $\dot{d}$ are held constant (Fig. 9c). Steady state glacier length also increases with $\dot{d}$ when $\dot{d}_{loc}$ and $\dot{d}_{width}$ are held constant

TCD
9, 6423–6470, 2015

(Fig. 9d). Increasing either $\dot{d}$ or $\dot{d}_{\text{width}}$ effects the system similarly (Fig. 9c and d). The dependence of glacier length on $\dot{d}$ and $\dot{d}_{\text{width}}$ is not linear (Fig. 9). If we combine the effects of $\dot{d}$ and $\dot{d}_{\text{width}}$ by comparing the d_{flux} with steady state glacier length we see that steady state glacier length is primarily dependent on d_{flux} (Fig. 9e). Length enhancement by a factor of 2 or more is viable for the range of d_{flux} explored.

4.3 Parameter sensitivity

We explore the sensitivity of the model to changes in h_* and ϕ using the base parameter set for other parameters and inputs. We vary h_* and ϕ, impose a step change increase in debris input to the ssdf glacier and compare the resulting steady state glacier lengths (Fig. 10). Simulated glacier length is highly sensitive to h_* (Fig. 10). For the same debris delivery variables, the more rapidly the melt rate is damped by debris (lower h_*), the longer the steady state glacier. Steady state debris-covered glacier length varies from 140 to 250 % of L_{ssdf} when h_* is varied from the extremes of 0.0035 to 0.165 m (160–215 % for the 1σ range (0.037–0.095 m)). Glacier length is not as sensitive to the choice of debris porosity, ϕ (Fig. 10). Variation of ϕ between the extreme range of 0 and 0.45 leads to lengths that range from 160 to 195 % extension from L_{ssdf}.

4.4 Comparison of model results with remote sensing derived data

Our model results show that steady, high debris fluxes onto glaciers lead to glacier lengthening and high percentages of debris cover (Figs. 8 and 9). Remote-sensing derived measurements of u_{surf} and AAR provide insight into valley glacier response to debris. We compare our model results to Scherler et al., (2011b)'s inventory of 287 debris-covered glacier surface velocities, AARs, and debris cover percentages from High Asia.

Scherler et al. (2011b) noted that debris cover percentage on glaciers correlates with steep above-glacier hillslopes. Because hillslope erosion rates and the percentage of

TCD
9, 6423–6470, 2015

exposed bedrock in the headwall increase with steeper slopes, it follows that increased debris input onto the glacier should also increase glacier length and the percentage of the glacier covered with debris. Our steady state model results confirm this inference and show how changes in debris input variables can capture first-order trends from real debris-covered glaciers (Fig. 11).

Scherler et al. (2011b) showed that large debris cover percentages correspond with small AARs outside the typical range of 0.5–0.7 seen on debris-free glaciers (e.g., Meier and Post, 1979). In our model simulations, increases in d_{flux} lead to increases in both steady state glacier length, and fractional debris cover (Fig. 11a). With a fixed ELA, the AAR must therefore decrease with an increased d_{flux} (Fig. 11a). Varying h_* (using the base parameter set with no changes in d_{flux} or $\dot{d}_{\text{loc}}$; Fig. 10) has a similar effect to varying d_{flux} (Fig. 11c and d). Changes in $\dot{d}_{\text{loc}}$ lead to small changes in AAR but considerable changes in fractional debris cover (Fig. 11a).

Scherler et al. (2011b) also showed that debris cover percentage correlated with the ratio of average u_{surf} from the lower half of glaciers to the average u_{surf} from the upper half of glaciers. Increasing d_{flux} leads to lower u_{surf} in the lower half of glaciers relative to u_{surf} in the upper half of glaciers (Fig. 11b). Changing the location of debris input, $\dot{d}_{\text{loc}}$, leads to small changes in the ratio of average u_{surf} but leads to large changes in the percentage of the glacier covered with debris.

While the simulations plot within the data from Scherler et al. (2011b), our steady state model results do not account for the full data spread (Fig. 11a). Our ssdf glacier has an AAR of 0.5. Adding debris to the model only reduces AARs. Simulations with initial ssdf glaciers with higher AARs could reproduce more of the data. The Scherler dataset was collected from glaciers responding to periods of negative mass balance. Reduced surface velocities under debris cover (not necessarily stagnant) – resulting from debris-covered glacier response to climate change – could account for the data with low debris cover percentages and low ratios of half length mean ice surface velocities (Fig. 11b).

TCD
9, 6423–6470, 2015

Changing the linear bed slope leads to similar relationships between debris cover %, AAR, and surface velocity to the simulations using the base bed slope. Notable differences occur primarily when the bed slope is reduced (Fig. 11c and d). With a reduced bed slope the initial debris-free steady state glacier is 3 times longer than the ssdf glacier. Even with the same hillslope debris fluxes as the simulations in Fig. 11a and b, the reduced bed slope leads to reduced asymmetry in the steady state debris-covered glacier surface velocities (Fig. 11d). The specific relationship of glacier response to debris is therefore also dependent on glacier size, bed slope, and the environmental mass balance gradient.

This model-data comparison shows that viable changes in debris flux, debris deposition location, and h_* can cause changes in debris cover percentage, AAR, and glacier surface velocities that correspond with patterns observed from real debris-covered glaciers. This lends support to the viability to our model framework, while also providing quantitative, theoretical support to previous data-based inferences.

5 Discussion

We explored the sensitivity of a new debris-covered glacier model to changes in various parameters and debris input related variables. Simulated glacier lengths are most sensitive to hillslope debris flux and the selection of the characteristic debris thickness. The location of debris deposition is important but plays a secondary role in setting glacier length. The time evolution of debris-covered glacier length is highly dependent on $d_{\text{flux}}^{\text{snout}}$, although steady state glacier length is not. Thick debris cover on glaciers from consistent debris input, independent of climate change tends to (1) reverse and reduce mass balance gradients; (2) extend glaciers; (3) reduce AARs; and (4) reduce gradients of ice discharge, ice thickness, and surface velocity under debris cover. Our model reproduces first-order relationships between debris cover percentages, AAR, and debris-perturbed surface velocity patterns from High Asian debris-covered glaciers.

TCD
9, 6423–6470, 2015

5.1 The importance of debris flux and h_* on steady state glacier length

Increases in hillslope debris flux (d_{flux}) lead to glacier extension (Figs. 8 and 9; Scherler et al., 2011b). But the rate and location of debris delivery to the surface ought to vary widely due to local geologic and climatic settings. Our simulations show that the flux of debris to the glacier surface, d_{flux}, is more important in determining the steady state debris-covered glacier length than $\dot{d}$, $\dot{d}_{\text{loc}}$, or $\dot{d}_{\text{width}}$ (Fig. 9). Debris delivery processes to the glacier surface (e.g., deposition by avalanches, rockfall, the melt out of debris septa forming ice-stream interaction medial moraines, etc.) are first-order controls on the geometry of debris deposits on glaciers. Because d_{flux} trumps the importance of $\dot{d}$, $\dot{d}_{\text{loc}}$, and $\dot{d}_{\text{width}}$, the specific debris delivery pathway may be secondary to the debris flux in determining glacier length.

The effects of changing h_* are similar to the effects of varying the hillslope debris flux (Figs. 10 and 11). Establishing the importance of d_{flux} for individual glaciers requires that we constrain the variability of h_* from glacier to glacier: small changes in h_* can lead to large changes in steady state glacier length (Fig. 10). Simulations using an exponential debris thickness-melt curve resulted in unrealistically long glaciers due to the rapid asymptote of melt towards zero. The hyperbolic parameterization is more physically defensible than the exponential parameterization if we assume that heat is transferred through debris by conduction.

Many paleoclimate estimates derived from glacial moraines neglect the potential effects of surface debris. Because debris can have a strong effect on glacier length, independent of climate change, debris should be considered amongst temperature and precipitation as primary controls of paleoglacier lengths (e.g., Clark et al., 1994; Scherler, et al., 2011b). The effect of debris on paleoclimate estimates can be mitigated by avoiding de-glaciated catchments with high-relief headwalls and supraglacially sourced moraine sediments.

TCD
9, 6423–6470, 2015

5.2 The effect of steady debris input on patterns of Q, H and u_{surf}

In all debris-perturbed simulations, the mass balance gradient down-glacier from the location of initial debris emergence, $\dot{e}_{x_{int}}$, reverses relative to the debris-free profile, decreases toward zero, and becomes more uniform (excluding the toe cell; Fig. 5). This reversal results in a reduction of the surface mass balance b' relative to the ssdf glacier (Fig. 6). Reducing b' toward zero reduces ice discharge gradients. The glacier must extend in order to reach a steady state.

Thick debris reduces b' toward 0 and also makes b' more uniform (Fig. 5). This leads to ice discharge gradients that are reduced toward zero and become more uniform near the terminus (Fig. 5). Because $Q = H\bar{u}$, the surface velocity pattern follows a similar concave up pattern near the terminus where ice thicknesses are small and b' is close to zero (Fig. 6). Low ice thicknesses and thick debris near the terminus leads to low, nearly uniform surface velocities, independent of climate change (Fig. 6). While it is possible that debris cover can produce low velocity portions of glaciers independent of climate change, periods of negative mass balance can lead to extensive portions of debris-covered glaciers with low surface velocities due to the largest increases in melt rates occurring near $\dot{e}_{x_{int}}$ (e.g., Kirkbride et al., 1993).

The ice discharge at $\dot{e}_{x_{int}}$ controls the steady state glacier length and the down glacier patterns of ice discharge, ice thickness and u_{surf}. In steady state, ice discharge at $\dot{e}_{x_{int}}$ represents the volume of ice per unit time that must be ablated between $\dot{e}_{x_{int}}$ and the terminus. Holding other debris related variables constant, if debris emerges where ice discharge is large, the glacier will extend further because more glacier surface under thick debris (where melt rates are more uniform) is needed to ablate and match the large ice discharge at $\dot{e}_{x_{int}}$. If debris emerges where ice discharge is small the glacier does not extend as far because less area is needed under debris to match ice discharge at $\dot{e}_{x_{int}}$ (Fig. 6). The location of debris deposition/emergence relative to the ELA is therefore an important variable in the debris-glacier system as it controls

TCD
9, 6423–6470, 2015

the relationship between debris cover percentage, AAR, and the pattern of surface velocities (Fig. 11).

The specific terminal pattern of ice discharge and thickness is controlled by the rate of debris removal from the toe. If $d_{\text{flux}}^{\text{snout}}$ is high an ice cliff may persist at the toe leading to high melt rates and the pre-mature termination of a glacier when compared to a glacier with a low $d_{\text{flux}}^{\text{snout}}$. If the magnitude of $d_{\text{flux}}^{\text{snout}}$ is low then the toe maybe drowned in debris, and the glacier may never reach steady state even with a steady climate. The glacier would continue to accumulate debris and slowly advance down valley with a slightly positive net mass balance (e.g., Konrad and Humphrey, 2000). It may be useful to consider if individual debris-covered glaciers are accumulating debris mass through time, losing debris mass through time, or potentially in steady state with regard to debris (Fig. 4).

The response time of the modeled glaciers is therefore dependent on the parameterization of $d_{\text{flux}}^{\text{snout}}$ (Appendix B). A glacier with rapid debris removal at the toe will tend to reach a steady state much faster than a glacier with slow debris removal from the toe (Appendix B). Documenting the rates of debris removal at the toe is vital for modeling and understanding individual debris-covered glacier response.

In our steady state simulations, the ice thickness is increased up-glacier from the point of debris emergence, $\dot{e}_{x_{\text{int}}}$ (Fig. 6). The thickness perturbations caused by emerging debris are diffused up glacier, leading to lower ice surface slopes and greater ice thicknesses than on debris-free glaciers of comparable sizes. The emergence of debris on a glacier can therefore perturb ice thickness both up and down glacier from $\dot{e}_{x_{\text{int}}}$. Debris cover decreases the surface mass balance and therefore also reduces the vertical component of englacial velocity; this leads to flow paths that are increasingly parallel to the surface (Konrad and Humphrey, 2000). Reducing ice melt rates results in lower debris emergence rates, leading to the further advection of debris down-glacier and expansion of the zone of debris emergence (Fig. 5a). Debris emergence zones on real glaciers will therefore tend to be wider than debris deposition zones.

TCD
9, 6423–6470, 2015

6 Future work

While we have explored first-order connections between glacier dynamics and debris deposition, additional components require investigation. Modeling the response of debris-covered glaciers to climate is the most pressing. The steady state results presented here can serve as initial conditions for future simulations exploring the response of debris-covered glaciers to climate change. Future efforts should also explore the importance of glacier size, environmental mass balance gradient, and bed slope as they modulate the effect of debris on glacier response.

We assumed a steady debris input for simplicity. In reality, hillslope erosion in high-relief settings occurs through thresholded, mass wasting processes. The effect of temporal and spatial changes in debris deposition must be addressed through both empirical and theoretical approaches. Isolated, large landslides have been shown to suppress melt rates, change glacier surface slopes and perturb glacier surface velocity fields (Gardner and Hewitt, 1990; Reznichenko et al., 2011; Shugar et al., 2012). If debris inputs are allowed to vary in space and time, a complex glacier length history will likely result even with a steady climate. The specifics of that history will depend strongly on the frequency and magnitude of mass wasting events and to a lesser degree the ice discharge at the point of debris emergence.

Our modeling did not account for the planview dimension of glaciers. Debris advected into the glacier between tributaries emerges to form ice-stream interaction medial moraines. While the spatial widening of such moraines has been addressed (Anderson, 2000), the merging of these medial moraines results in debris thickening that we do not account for. Our present work lays the framework for such a 2-D planview model.

Ice cliffs and surface ponds are neglected in this study for simplicity but should be included in numerical models of glacier response to debris and climate change (e.g., Benn et al., 2012). Planview modeling of debris-covered glacier response is also needed (e.g., Menounos, et al., 2013). The melt-enhancing effects of thin debris covers should be included in future modeling efforts. Environmental mass balance profiles

TCD
9, 6423–6470, 2015

and snow lines are not steady from year-to-year. The response of debris-covered glaciers to interannual climate variability must also be explored (Roe and O'Neal, 2009; Anderson et al., 2014). Debris covers and glacier lengths will fluctuate in response to this variability because of the feedbacks between the debris emergence, ice dynamics, and climate.

Debris advection through and on a glacier can take hundreds of years, leading to memory in the system. The response of individual debris-covered glaciers to climate change is therefore dependent on the distribution of debris on and in the glacier when the climate change occurs. Further constraint of englacial and surface debris is needed to understand the decadal to centennial response of debris-covered glaciers to climate change.

7 Conclusions

Before modeling the response of debris-covered glaciers to a warming climate, it is necessary to constrain how debris effects glaciers – independent of climate change. We provide a new framework to explore debris-covered glacier evolution and explore valley glacier sensitivity to debris input. Our simulations show that:

- Thick debris cover tends to reduce gradients of ice discharge, ice thickness, and surfaces velocities, independent of climate change.
- Debris-covered glacier length is highly sensitive to debris flux to the glacier surface. High surface debris fluxes can greatly increase glacier lengths relative to glaciers responding to the same climate without debris. Increases in debris flux lead to smaller AARs and larger debris covered fractions. Changes in the debris deposition zone width or the debris deposition rate are secondary to the total surface debris flux in governing the glacier geometry. This model provides a framework to quantify the effect of debris input on glacier length, and can

TCD
9, 6423–6470, 2015

therefore be used to estimate the effect of debris input on paleoclimate estimates derived from glacier models.

- The site of supraglacial debris deposition relative to the ELA modulates glacier response to debris. Steady debris input where ice discharge is high (near the ELA) leads to longer glaciers with greater fractional debris cover, whereas the same steady debris input where ice discharge is low (near the headwall or terminus) leads to shorter glaciers with smaller fractional debris cover.
- The importance of the mechanism of debris deposition onto glaciers (e.g., delivery by avalanching or by melt out of debris septa) is likely secondary to the importance of the total surface debris flux.
- Debris-covered glacier length is highly sensitive to the relationship between surface debris thickness and sub-debris melt. Our simulations support the use of capped hyperbolic debris thickness-melt curve fits (Eq. 3).
- The rate and process of debris removal from the terminus exerts strong control on the time evolution of debris-covered glaciers, but only weakly controls the eventual steady-state length.
- Debris cover can perturb ice thicknesses and glacier surface slopes up-glacier from the debris-covered portion of the glacier. Thick debris cover can expand the zone of debris emergence. Debris deposition zones will therefore be more narrow than zones of debris emergence.

Glacier response to debris cover is most sensitive to surface debris flux. Our ability to predict the response of debris-covered glaciers to climate change, and to extract paleoclimate estimates from moraines in high-relief settings, is therefore highly dependent on our constraint of surface debris fluxes in the future and the past.

TCD
9, 6423–6470, 2015

Appendix A

In our model, the debris thickness $h_{\text{debris}}(x,t)$ represents a layer of equal thickness on any cell. There is therefore a timescale built into the thickening of debris in a cell that is dependent on dx. Increasing dx from 100 to 200 m leads to differences in steady state debris-covered glacier length that are less than 200 m even when debris flux is varied [=]. Because melt (Fig. 3) is highly sensitive to debris thickness, a newly formed glacier cell at the toe can be exposed to melt rates un-perturbed by debris. As a result, the simulated glacier can be trapped in a steady length, although large amounts of ice are melted without the protection of debris. To correct this, we implement a triangular terminus parameterization (after Budd and Jenssen, 1975; Waddington, 1981). The volume of the terminal triangle at time $t + \mathrm{d}t$ is the sum of the old snout volume, the ablated volume, and the volumetric flow past the last grid point. A single environmental melt rate is calculated based on the mean elevation of the toe, and ablation is calculated perpendicular to the surface of the triangle. Equation (16) and the surface length of the wedge define the debris thickness on the snout. When the snout length is greater than 2dx, the glacier advances to the next cell. If the snout is shorter than dx the glacier retreats one cell. Because the terminus parameterization allows the glacier to change length at the sub-dx scale, simulated glaciers avoid numerical traps and advance to true steady states. In this model, steady state occurs when $d_{\text{flux}} = d_{\text{flux}}^{\text{snout}}$ and the glacier length is steady.

Appendix B

Debris deposited on the glacier surface is removed from the glacier by ice cliff retreat or wasting down the terminal glacier slope. Unfortunately, the rates and processes of debris removal from glacier toes are poorly documented. We therefore explore parameterizations for the debris removal flux from the glacier ($d_{\text{flux}}^{\text{snout}}$) and their effect on glacier length (using the base parameter set where d_{flux} $\mathrm{m}^3\,\mathrm{m}^{-1}\,\mathrm{yr}^{-1}$). Each simulation

TCD
9, 6423–6470, 2015

starts with the ssdf glacier followed by a step change increase in d_{flux}. We consider $d_{\text{flux}}^{\text{snout}} = c$, $d_{\text{flux}}^{\text{snout}} = ch_{\text{debris}}$, and $d_{\text{flux}}^{\text{snout}} = c\dot{b}_z h_{\text{debris}}$ where c is a constant that ranges between 0.1 and 10 and variable units such that $d_{\text{flux}}^{\text{snout}}[=]\,\text{m}^3\,\text{m}^{-1}\,\text{yr}^{-1}$. Independent of the parameterization, $d_{\text{flux}}^{\text{snout}}$ controls both the time needed to reach steady state as well as whether a simulated glacier can reach steady state (Fig. B1).

Large changes in $d_{\text{flux}}^{\text{snout}}$ lead to minor changes in glacier length even after 5000 years, implying that the choice of the $d_{\text{flux}}^{\text{snout}}$ parameterization would have a minor effect on the length results presented (Fig. B1). All three parameterizations lead to the same steady state length for low c values (190 % of L_{ssdf}).

If $d_{\text{flux}}^{\text{snout}}$ cannot evolve to a state where $d_{\text{flux}}^{\text{snout}} = d_{\text{flux}}$, surface debris thickens unrealistically and the glacier never reaches steady state. For $d_{\text{flux}}^{\text{snout}} = c$ the glacier will never reach steady state if c is less than $3.2\,\text{m}^3\,\text{m}^{-1}\,\text{yr}^{-1}$. For $d_{\text{flux}}^{\text{snout}} = ch_{\text{debris}}$, and $d_{\text{flux}}^{\text{snout}} = c\dot{b}_z h_{\text{debris}}$ the value of $d_{\text{flux}}^{\text{snout}}$ changes through each simulation based on the debris thickness on the toe and the local debris-free melt rate. The $d_{\text{flux}}^{\text{snout}} = c\dot{b}_z h_{\text{debris}}$ parameter shows a wider length variation than the $d_{\text{flux}}^{\text{snout}} = ch_{\text{debris}}$ parameterization because $d_{\text{flux}}^{\text{snout}} = c\dot{b}_z h_{\text{debris}}$ results in a wider range of $d_{\text{flux}}^{\text{snout}}$ values due to the $\dot{b}_z$ term. To insure that steady state can be achieved in each simulation, we include the melt rate term in the $d_{\text{flux}}^{\text{snout}}$ parameterization (Fig. B1) that codifies an assumption that debris removal processes at the toe are in some fashion dependent on local air temperature and hence melt rates. We use $d_{\text{flux}}^{\text{snout}} = c\dot{b}_z h_{\text{debris}}$ for all simulations outside of this Appendix (with $c = 1$).

Acknowledgements. This research was partially supported by NSF grant DGE-1144083 (GRFP) to LSA and NSF grant EAR-1123855 to RSA. The writing and modeling benefitted significantly from comments on an earlier draft by G. Roe, H. Rajaram, and D. Scherler.

TCD
9, 6423–6470, 2015

References

Anderson, L. S.: Glacier response to climate change: modeling the effects of weather and debris-cover, PhD thesis, University of Colorado, Boulder, 2014.

Anderson, L. S., Roe, G. H., and Anderson, R. S.: The effects of interannual climate variability on the moraine record, Geology, 42, 55–58, 2014.

Anderson, R. S.: A model of ablation-dominated medial moraines and the generation of debris-mantled glacier snouts, J. Glaciol., 46, 459–469, doi:10.3189/172756500781833025, 2000.

Arsenault, A. M. and Meigs, A. J.: Contribution of deep-seated bedrock landslides to erosion of a glaciated basin in southern Alaska, Earth Surf. Proc. Land., 30, 1111–1125, doi:10.1002/esp.1265, 2005.

Ballantyne, C. K. and Harris, C.: The Periglaciation of Great Britain, Cambridge University Press, Cambridge, UK, 1994.

Banerjee, A. and Shankar, R.: On the response of Himalayan glaciers to climate change, J. Glaciol., 59, 480–490, 2013.

Benn, D. and Evans, D. J. A.: Glaciers and Glaciation, Routledge, London, UK, 2010.

Benn, D. I. and Owen, L. A.: Himalayan glacial sedimentary environments: a framework for reconstructing and dating the former extent of glaciers in high mountains, Quatern. Int., 97–98, 3–25, doi:10.1016/S1040-6182(02)00048-4, 2002.

Benn, D., Bolch, T., Hands, K., Gulley, J., Luckman, A., Nicholson, L., Quincey, D., Thompson, S., Toumi, R., and Wiseman, S.: Response of debris-covered glaciers in the Mount Everest region to recent warming, and implications for outburst flood hazards, Earth-Sci. Rev., 114, 156–174, doi:10.1016/j.earscirev.2012.03.008, 2012.

Bolch, T., Pieczonka, T., and Benn, D. I.: Multi-decadal mass loss of glaciers in the Everest area (Nepal Himalaya) derived from stereo imagery, The Cryosphere, 5, 349–358, doi:10.5194/tc-5-349-2011, 2011.

Boulton, G. S. and Eyles, N.: Sedimentation by valley glaciers: a model and genetic classification, Moraines and Varves, 33, 11–23, 1979.

Bozhinskiy, A. N., Krass, M. S., and Popovnin, V. V.: Role of debris cover in the thermal physics of glaciers, J. Glaciol., 32, 255–266, 1986.

Brook, M., Hagg, W., and Winkler, S.: Debris cover and surface melt at a temperate maritime alpine glacier: Franz Josef Glacier, New Zealand, New Zeal. J. Geol. Geop., 56, 27–38, doi:10.1080/00288306.2012.736391, 2013.

TCD
9, 6423–6470, 2015

Budd, W. and Jenssen, D.: Numerical modelling of glacier systems, IAHS-AISH P., 104, 257–291, 1975.
Clark, D. H., Clark, M. M., and Gillespie, A. R.: Debris-covered glaciers in the Sierra Nevada, California, and their implications for snowline reconstructions, Quaternary Res., 41, 139–153, 1994.
Conway, H. and Rasmussen, L. A.: Summer temperature profiles within supraglacial debris on Khunibu Glacier, Nepal, in: Debris-covered Glaciers: Proceedings of an International Workshop Held at the University of Washington in Seattle, Washington, USA, 13–15 September 2000, 264, p. 89, IAHS, 2000.
Cuffey, K. and Paterson, W.: The Physics of Glaciers, Elsevier, Oxford, UK, 4th edn., 2010.
Deline, P.: Interactions between rock avalanches and glaciers in the Mont Blanc massif during the late Holocene, Quaternary Sci. Rev., 28, 1070–1083, doi:10.1016/j.quascirev.2008.09.025, 2009.
Eyles, N. and Rogerson, R. J.: A framework for the investigation of medial moraine formation: Austerdalsbreen, Norway, and Berendon Glacier, British Columbia, Canada, J. Glaciol., 20, 99–113, 1978.
Fyffe, C. L.: The hydrology of debris-covered glaciers, PhD thesis, University of Dundee, UK, 2012.
Gardner, J. S. and Hewitt, K.: A surge of Bualtar Glacier, Karakoram Range, Pakistan: a possible landslide trigger, J. Glaciol., 36, 159–162, 1990.
Hagg, W., Mayer, C., Lambrecht, A., and Helm, A.: Sub-debris melt rates on Southern Inylchek Glacier, Central Tian Shan, Geogr. Ann. A, 90, 55–63, 2008.
Heimsath, A. M. and McGlynn, R.: Quantifying periglacial erosion in the Nepal high Himalaya, Geomorphology, 97, 5–23, doi:10.1016/j.geomorph.2007.02.046, 2008.
Hooke, R. L. and Hudleston, P. J.: Origin of foliation in glaciers, J. Glaciol., 20, 285–299, 1978.
Humlum, O.: The geomorphic significance of rock glaciers: estimates of rock glacier debris volumes and headwall recession rates in West Greenland, Geomorphology, 35, 41–67, 2000.
Humlum, O.: Holocene permafrost aggradation in Svalbard, Geological Society, London, Special Publications, 242, 119–129, doi:10.1144/GSL.SP.2005.242.01.11, 2005.
Kayasha, R., Takeuchi, Y., Nakawo, M., and Ageta, Y.: Practical prediction of ice melting beneath various thickness of debris cover on Kliumbu Glacier, Nepal, using a positive degree-day factor, in: Debris-covered Glaciers: Proceedings of an International Workshop Held at the

TCD
9, 6423–6470, 2015

University of Washington in Seattle, Washington, USA, 13–15 September 2000, 264, p. 71, IAHS, IAHS Publication, 2000.
Kessler, M. A., Anderson, R. S., and Stock, G. M.: Modeling topographic and climatic control of east-west asymmetry in Sierra Nevada glacier length during the Last Glacial Maximum, J. Geophys. Res., 111, F02002, doi:10.1029/2005JF000365, 2006.
Khan, M. I.: Ablation on Barpu glacier, Karakoram Himalaya, Pakistan a study of melt processes on a faceted, debris-covered ice surface, PhD thesis, Wilfrid Laurier University, USA, 1989.
Kirkbride, M. P.: The temporal significance of transitions from melting to calving termini at glaciers in the central Southern Alps of New Zealand, Holocene, 3, 232–240, doi:10.1177/095968369300300305, 1993.
Kirkbride, M. P.: Debris-covered glaciers, in: Encyclopedia of snow, ice and glaciers, edited by: Singh, V., Singh, P., and Haritashya, U. K., Springer, Dordrecht, 190–191, 2011.
Kirkbride, M. P. and Deline, P.: The formation of supraglacial debris covers by primary dispersal from transverse englacial debris bands, Earth Surf. Proc. Land., 38, 1779–1792, doi:10.1002/esp.3416, 2013.
Konrad, S. K. and Humphrey, N. F.: Steady-state flow model of debris-covered glaciers (rock glaciers), in: Debris-covered Glaciers: Proceedings of an International Workshop Held at the University of Washington in Seattle, Washington, USA, 13–15 September 2000, 255–266, 2000.
Loomis, S. R.: Morphology and ablation processes on glacier ice. Part 1, Morphology and structure of an ice-cored medial moraine, Kaskawulsh Glacier, Yukon, Arctic Institute of North America, Research Paper, 1–65, 1970.
Lukas, S., Nicholson, L. I., Ross, F. H., and Humlum, O.: Formation, meltout processes and landscape alteration of high-Arctic ice-cored moraines examples from Nordenskiold Land, Central Spitsbergen, Polar Geography, 29, 157–187, doi:10.1080/789610198, 2005.
Lundstrom, S. C.: The budget and effect of superglacial debris on Eliot Glacier, Mount Hood, Oregon, PhD thesis, University of Colorado, Boulder, 1993.
MacGregor, K. R., Anderson, R. S., and Waddington, E. D.: Numerical simulations of glacial-valley longitudinal profile evolution, Geology, 28, 1031–1034, 2000.
Marshall, S. J., Bjornsson, H., Flowers, G. E., and Clarke, G. K. C.: Simulation of Vatnajökull ice cap dynamics, J. Geophys. Res., 110, 126–135, doi:10.1029/2004JF000262, 2005.
Mattson, L. E., Gardner, J. S., and Young, G. J.: Ablation on debris covered glaciers: an example from the Rakhiot Glacier, Punjab, Himalaya, in: Snow and Glacier Hydrology (Proceedings of

TCD
9, 6423–6470, 2015

the Kathmandu Symposium), Kathmandu, November 1992, IAHS Publication, 218, 289–296, 1993.
Meier, M. and Post, A.: Recent Variations in mass net budgets of glaciers in western North America, IASH-AISH P., 58, 63–77, 1962.
Menounos, B., Clague, J. J., Clarke, G. K. C., Marcott, S. A., Osborn, G., Clark, P. U., Tennant, C., and Novak, A. M.: Did rock avalanche deposits modulate the late Holocene advance of Tiedemann Glacier, southern Coast Mountains, British Columbia, Canada?, Earth Planet. Sc. Lett., 384, 154–164, 2013.
Messerli, B. and Zurbuchen, M.: Block-gletscher im Weissmies und Aletsch und ihre photogrammetrische Kartierung, Die Alpen, 3, 139–152, 1968.
Mihalcea, C., Mayer, C., Diolaiuti, G., Lambrecht, A., Smiraglia, C., and Tartari, G.: Ice ablation and meteorological conditions on the debris-covered area of Baltoro glacier, Karakoram, Pakistan, Ann. Glaciol., 43, 292–300, 2006.
Molnar, P., Anderson, R. S., and Anderson, S. P.: Tectonics, fracturing of rock, and erosion, J. Geophys. Res.-Earth, 112, 1–12, doi:10.1029/2005JF000433, 2007.
Naito, N., Nakawo, M., Kadota, T., and Raymond, C. F.: Numerical simulation of recent shrinkage of Khuinbu Glacier, Nepal Himalayas, in: Debris-covered Glaciers: Proceedings of an International Workshop Held at the University of Washington in Seattle, Washington, USA, 13–15 September 2000, 264, p. 245, IAHS, 2000.
Nicholson, L. and Benn, D. I.: Calculating ice melt beneath a debris layer using meteorological data, J. Glaciol., 52, 463–470, 2006.
Nye, J. F.: A numerical method of inferring the budget history of a glacier from its advance and retreat, J. Glaciol., 5, 589–607, 1965.
Østrem, G.: Ice melting under a thin layer of moraine, and the existence of ice cores in moraine ridges, Geogr. Ann. Ser. A, Phys. Geogr., 228–230, 1959.
Oerlemans, J.: An attempt to simulate historic front variations of Nigardsbreen, Norway, Theor. Appl. Climatol., 135, 126–135, 1986.
O'Farrell, C. R. O., Heimsath, A. M., Lawson, D. E., Jorgensen, L. M., Evenson, E. B., Larson, G., and Denner, J.: Quantifying periglacial erosion: insights on a glacial sediment budget, Matanuska Glacier, Alaska, Earth Surf. Proc. Land., 34, 2008–2022, 2009.
Ouimet, W. B., Whipple, K. X., and Granger, D. E.: Beyond threshold hillslopes: channel adjustment to base-level fall in tectonically active mountain ranges, Geology, 37, 579–582, doi:10.1130/G30013A.1, 2009.

TCD
9, 6423–6470, 2015

Owen, L. A. and Derbyshire, E.: The Karakoram glacial depositional system, Z. Geomorphol. Supp., 76, 33–73, 1989.
Owen, L. A., Derbyshire, E., and Scott, C. H.: Contemporary sediment production and transfer in high-altitude glaciers, Sediment. Geol., 155, 13–36, 2003.
Raper, S. C. B. and Braithwaite, R. J.: Low sea level rise projections from mountain glaciers and icecaps under global warming, Nature, 439, 311–313, doi:10.1038/nature04448, 2006.
Reid, T. D. and Brock, B. W.: An energy-balance model for debris-covered glaciers including heat conduction through the debris layer, J. Glaciol., 56, 903–916, doi:10.3189/002214310794457218, 2010.
Reid, T. D. and Brock, B. W.: Assessing ice-cliff backwasting and its contribution to total ablation of debris-covered Miage glacier, Mont Blanc massif, Italy, J. Glaciol., 60, 3–13, 2014.
Reznichenko, N. V., Davies, T. R. H., and Alexander, D. J.: Effects of rock avalanches on glacier behaviour and moraine formation, Geomorphology, 132, 327–338, doi:10.1016/j.geomorph.2011.05.019, 2011.
Roe, G. H. and Neal, M. A. O.: The response of glaciers to intrinsic climate variability: observations and models of late-Holocene variations in the Pacific Northwest, J. Glaciol., 55, 839–854, 2009.
Scherler, D.: Climatic limits to headwall retreat in the Khumbu Himalaya, eastern Nepal, Geology, doi:10.1130/G35975.1, 2014.
Scherler, D., Bookhagen, B., and Strecker, M. R.: Spatially variable response of Himalayan glaciers to climate change affected by debris cover, Nat. Geosci., 4, 156–159, doi:10.1038/ngeo1068, 2011a.
Scherler, D., Bookhagen, B., and Strecker, M. R.: Hillslope-glacier coupling: the interplay of topography and glacial dynamics in High Asia, J. Geophys. Res., 116, F02019, doi:10.1029/2010JF001751, 2011b.
Shea, J. M., Immerzeel, W. W., Wagnon, P., Vincent, C., and Bajracharya, S.: Modelling glacier change in the Everest region, Nepal Himalaya, The Cryosphere, 9, 1105–1128, doi:10.5194/tc-9-1105-2015, 2015.
Shroder, J. F., Shroder, J. F., Bishop, M. P., Bishop, M. P., Copland, L., Copland, L., Sloan, V. F., and Sloan, V. F.: Debris-covered glaciers and rock glaciers in the Nanga Parbat Himalaya, Pakistan, Geogr. Ann. A, 82, 17–31, doi:10.1111/j.0435-3676.2000.00108.x, 2000.

TCD
9, 6423–6470, 2015

Shugar, D. H., Rabus, B. T., Clague, J. J., and Capps, D. M.: The response of Black Rapids Glacier, Alaska, to the Denali earthquake rock avalanches, J. Geophys. Res.-Earth, 117, 1–14, doi:10.1029/2011JF002011, 2012.

Smolarkiewicz, P. K.: A simple positive definite advection scheme with small implicit diffusion, Mon. Weather Rev., 111, 479–486, 1983.

Stock, J. D. and Montgomery, D. R.: Geologic constraints on bedrock river incision using the stream power law, J. Geophys. Res., 104, 4983, doi:10.1029/98JB02139, 1999.

Vacco, D. A., Alley, R. B., and Pollard, D.: Glacial advance and stagnation caused by rock avalanches, Earth Planet. Sc. Lett., 294, 123–130, doi:10.1016/j.epsl.2010.03.019, 2010.

Waddington, E. D.: Accurate modelling of glacier flow, PhD thesis, University of British Columbia, Canada, 1981.

Wagnon, P., Vincent, C., Arnaud, Y., Berthier, E., Vuillermoz, E., Gruber, S., Ménégoz, M., Gilbert, A., Dumont, M., Shea, J. M., Stumm, D., and Pokhrel, B. K.: Seasonal and annual mass balances of Mera and Pokalde glaciers (Nepal Himalaya) since 2007, The Cryosphere, 7, 1769–1786, doi:10.5194/tc-7-1769-2013, 2013.

Wang, L., Li, Z., and Wang, F.: Spatial distribution of the debris layer on glaciers of the Tuomuer Peak, western Tian Shan, J. Earth Sci., 22, 528–538, doi:10.1007/s12583-011-0205-6, 2011.

Ward, D. J. and Anderson, R. S.: The use of ablation-dominated medial moraines as samplers for 10Be-derived erosion rates of glacier valley walls, Kichatna Mountains, AK, Earth Surf. Proc. Land., 36, 495–512, doi:10.1002/esp.2068, 2011.

WGMS: Global glacier changes: facts and figures, edited by: Zemp, M., Roer, I., Kaab, A., Hoelzle, M., Paul, F., and Haerberli, W., UNEP, World Glacier Monitoring Service, Zürich, 2008.

TCD
9, 6423–6470, 2015

Table 1. Parameters definitions and values.

Parameter	Name	Min	Base	Max	Units
ELA	Equilibrium-line altitude		5000		m
$\frac{db_z}{dz}$	Surface mass balance gradient		0.0075		yr^{-1}
b_{cap}	Maximum accumulation		2		$m\,yr^{-1}$
Z_{max}	Maximum bed elevation		5200		m
α	Bed slope	4 %	8 %	20 %	
dt	Time step		0.01		yr
dx	Spatial discretization		100	200	m
g	Gravity		9.81		ms^{-2}
n	Glen's constant		3		
A	Flow law parameter		2.4×10^{-24}		$Pa^{-3}\,yr^{-1}$
f	Shapefactor		0.75		
U_c	Critical sliding speed		5		$m\,yr^{-1}$
τ_c	Reference basal shear stress		10^5		Pa
ρ_{ice}	Ice density		917		$kg\,m^{-3}$
m_z	# of cells per ice column		20		
ρ_{rock}	Debris density		2650		$kg\,m^{-3}$
h_*	Characteristic debris thickness	0.025	0.065	0.165	m
ϕ	Surface debris porosity	0	0.3	0.45	
$\dot{d}$	Debris deposition rate	1	8	8	$mm\,yr^{-1}$
$\dot{d}_{loc}$	Debris deposition location	7 %	42 %	98 %	
$\dot{d}_{width}$	Debris deposit width	100	400	1600	m
d_{flux}	Debris flux onto the glacier	0.1	3.2	6.4	$m^3\,m^{-1}\,yr^{-1}$
d_{flux}^{snout}	Debris flux off the glacier				$m^3\,m^{-1}\,yr^{-1}$
L_{ssdf}	Steady state debris-free glacier length		8700		m

TCD
9, 6423–6470, 2015

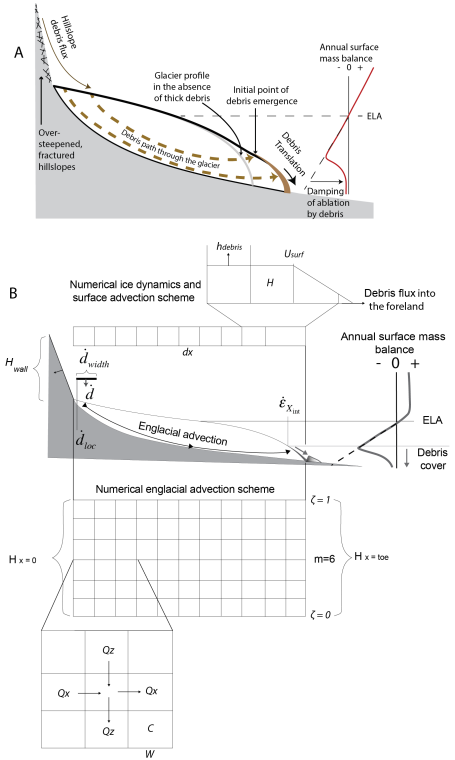

Figure 1. (a) Schematic of the debris-glacier system. Debris deposited on or emerging in the ablation zone reduces melt rates (above the critical thickness) leading to the reduction in gradients of ice discharge and the lengthening of glaciers. **(b)** Schematic of the coupled debris-glacier model. Debris deposited on the glacier is either advected through the glacier and/or advected down the glacier surface. Englacial debris is advected using 2-D rectangular grid and coordinate transform. Ice physics and supraglacial debris advection is treated on a 1-D grid.

TCD
9, 6423–6470, 2015

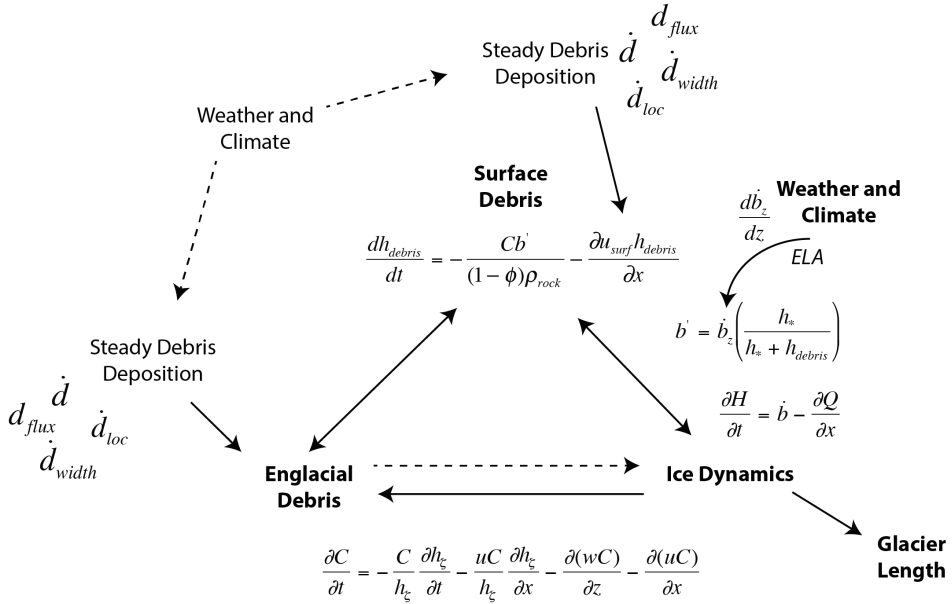

Figure 2. Flow chart of the elements connected in this debris-glacier model. Solid arrows represent the feedbacks we explore. Dashed arrows are neglected.

TCD
9, 6423–6470, 2015

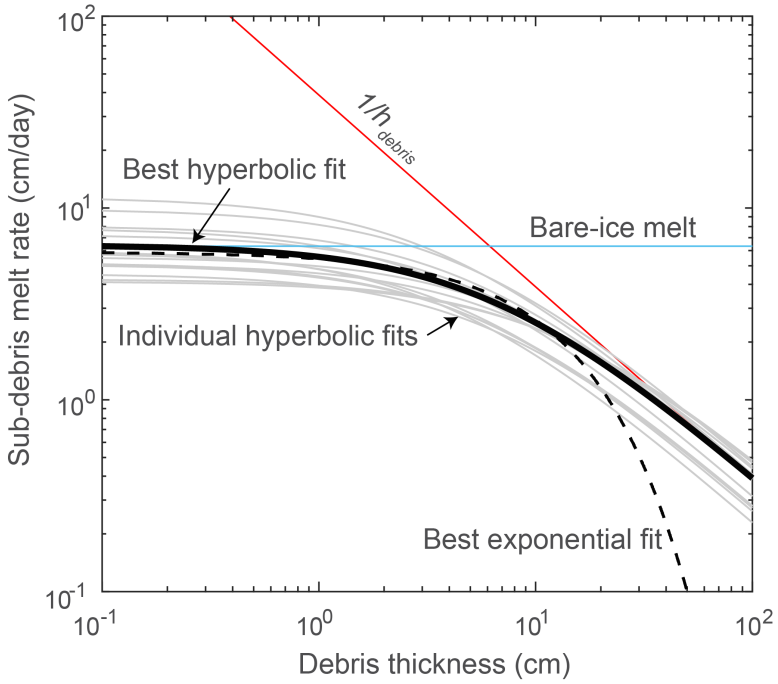

Figure 3. Compilation of curve fits to data from 15 melt rate vs. debris thickness studies (Østrem, 1959; Loomis, 1970; Khan, 1989; Mattson, et al., 1993; Lundstrom, 1993; Kayastha, et al., 2000; Lukas et al., 2005; Mihalcea, et al., 2006; Nicolson and Benn, 2006; Hagg, et al., 2008; Reid and Brock, 2010; Wang, 2011; Fyffe, 2012; Brook, et al., 2013; Anderson, 2014) (mean h_* is 0.066 ± 0.029 m (1σ), and ranges from 0.03 to 0.13 m). These curve fits are used to determine the parameter ranges in Table 1 for h_*. The best exponential fit is the mean of all the exponential curve fits; using sub-debris melt = $ae^{\frac{-h_{debris}}{b}}$ $a = 5.89\,\mathrm{cm\,day^{-1}}$, $b = 12.27$ cm.

TCD
9, 6423–6470, 2015

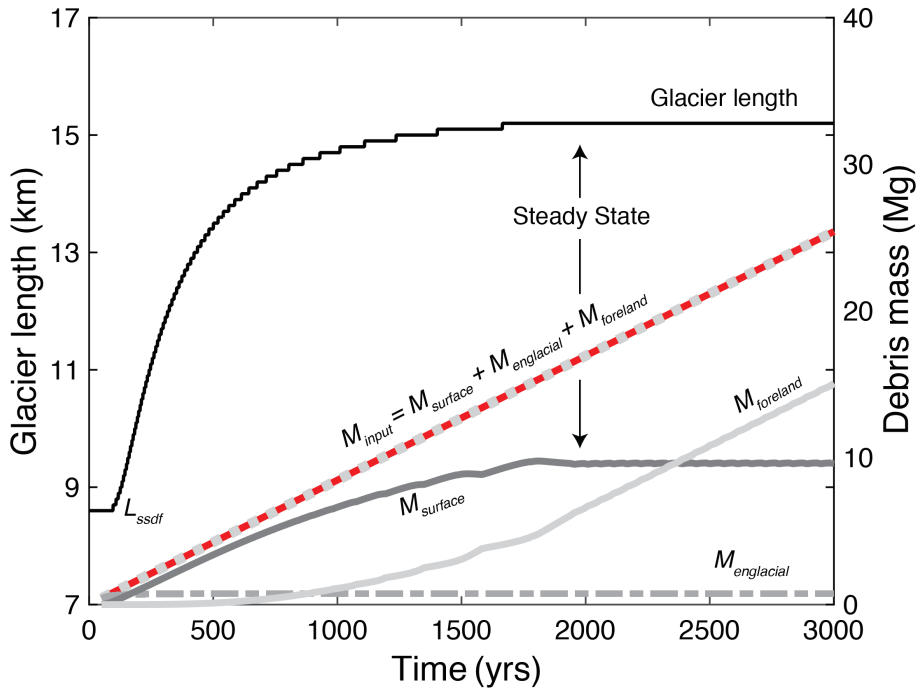

Figure 4. Debris mass vs. time. The englacial debris mass reaches steady state rapidly because debris is deposited near the ELA and englacial advection paths are short. As debris emerges in the ablation zone $M_{surface}$ increases nearly at the rate of debris input to the glacier. As the glacier nears a steady length the debris mass transferred to the glacier foreland increases. The glacier reaches steady state when $d_{flux} = d_{flux}^{snout}$ and the glacier length is steady (see Appendix A).

TCD
9, 6423–6470, 2015

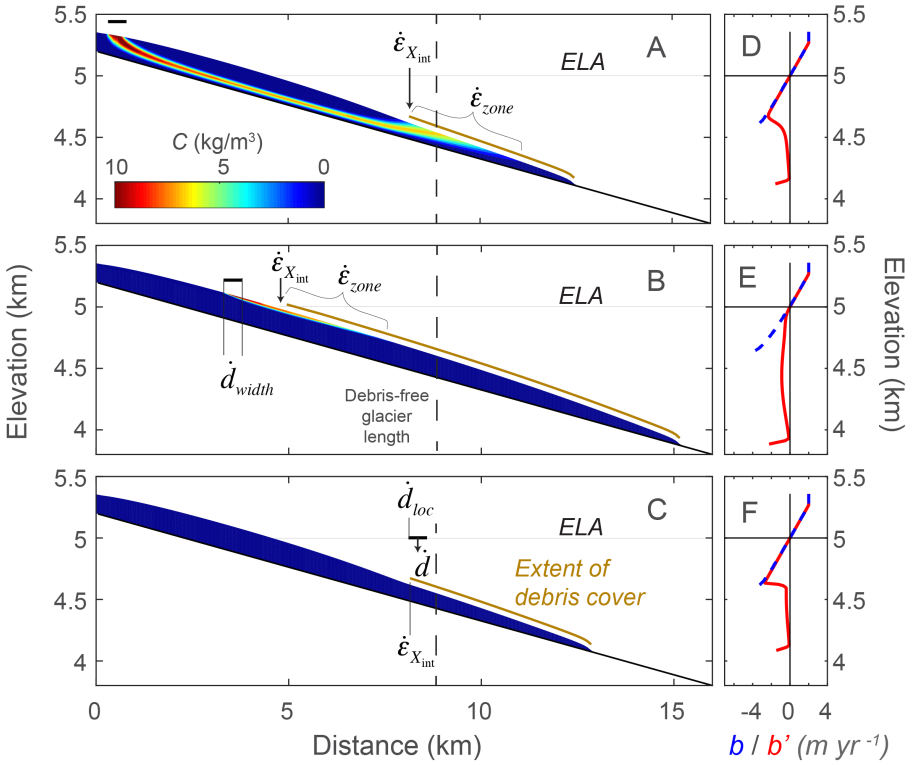

Figure 5. Modeled glacier changes due to changes in $\dot{d}_{loc}$ with $\dot{d}_*$ held constant. Englacial debris concentrations **(a–c)** and mass balance profiles **(d–f)** for three steady state debris-covered glacier simulations. $d_{flux} = 3.2\,m^3\,m^{-1}\,yr^{-1}$ for each panel. **(a)** $\dot{d}_{loc}$ is 7 % of L_{ssdf} from the head of the glacier. **(b)** $\dot{d}_{loc}$ is 42 % to L_{ssdf}. **(c)** $\dot{d}_{loc} = 98$ % to L_{ssdf}. The increase in melt rate near the toe is related to the thinning of debris due to the d^{snout}_{flux} parameterization. $\dot{\varepsilon}_{x_{int}}$ is the point of initial debris emergence and $\dot{\varepsilon}_{zone}$ is the length of the glacier over which englacial debris emerges.

TCD
9, 6423–6470, 2015

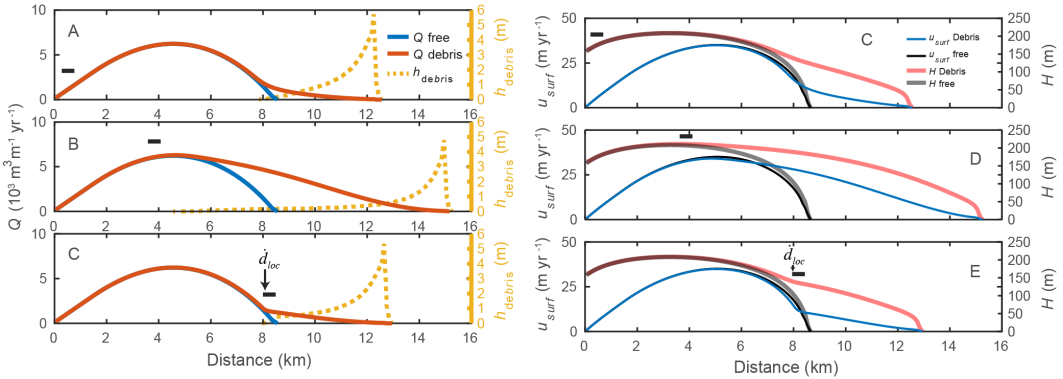

Figure 6. Modeled glacier changes due to changes in $\dot{d}_{loc}$. d_{flux} = 3.2 m^3 m^{-1} yr^{-1} for each panel and other parameters excluding $\dot{d}_{loc}$ are from the base set. **(a–c)** Comparison of h_{debris} and Q for the debris covered and debris free cases shown in Fig. 6. **(a)** $\dot{d}_{loc}$ is 7 % from the headwall to L_{ssdf}. **(b)** $\dot{d}_{loc}$ is 42 % from the headwall to L_{ssdf}. **(c)** $\dot{d}_{loc}$ is 98 % from the headwall to L_{ssdf}. **(d)** $\dot{d}_{loc}$ is 7 % from the headwall to L_{ssdf}. **(e)** $\dot{d}_{loc}$ is 42 % from the headwall to L_{ssdf}. **(f)** $\dot{d}_{loc}$ is 98 % from the headwall to L_{ssdf}.

TCD
9, 6423–6470, 2015

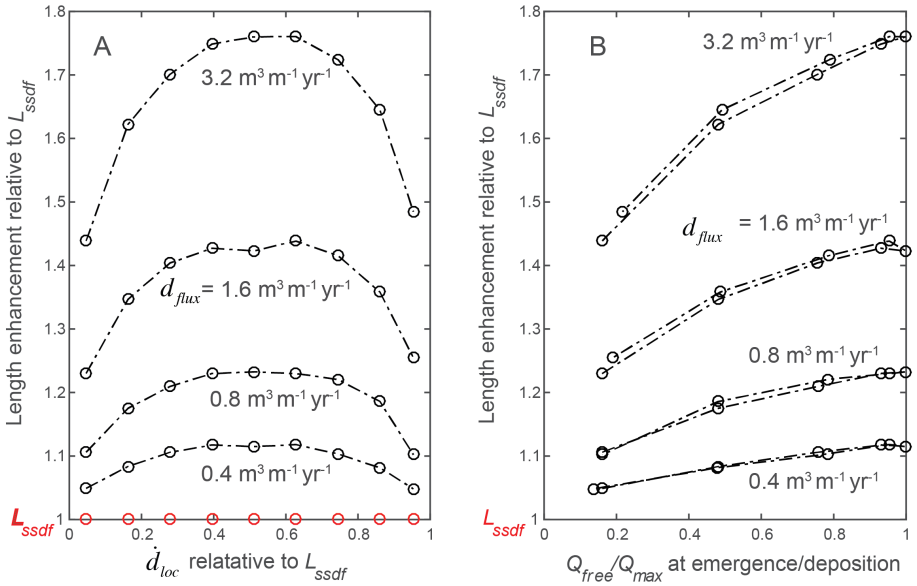

Figure 7. Glacier length variations with changes in d_{flux} and $\dot{d}_{\text{loc}}$. Modeled glacier length is normalized by L_{ssdf}. Each string of connected markers represents simulations with the same $\dot{d}$. The red markers indicate the ssdf glacier length. **(a)** Normalized glacier length relative to $\dot{d}_{\text{loc}}$. **(b)** Normalized glacier length relative to $Q_{\text{free}}/Q_{\text{max}}$ at the point of debris emergence/deposition.

TCD
9, 6423–6470, 2015

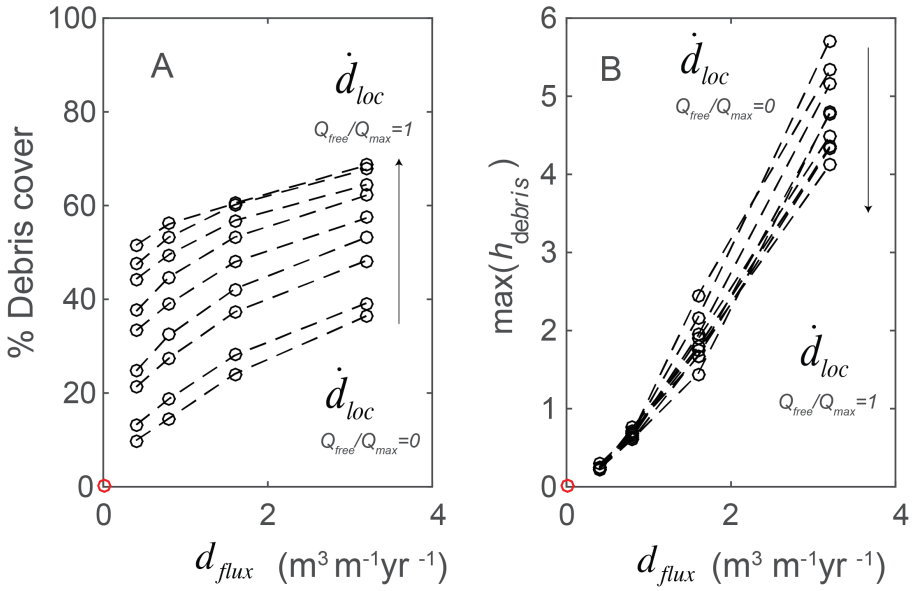

Figure 8. Debris related results from 36 simulations varying $\dot{d}_{loc}$ and d_{flux}. All black circles are derived from steady state debris-covered glaciers. Red circles show results from the debris-free glacier. **(a)** Dependence of debris cover percentage on d_{flux} and $\dot{d}_{loc}$. Dashed lines connect simulations with the same $\dot{d}_{loc}$. **(b)** Dependence of max(h_{debris}) on d_{flux}.

TCD
9, 6423–6470, 2015

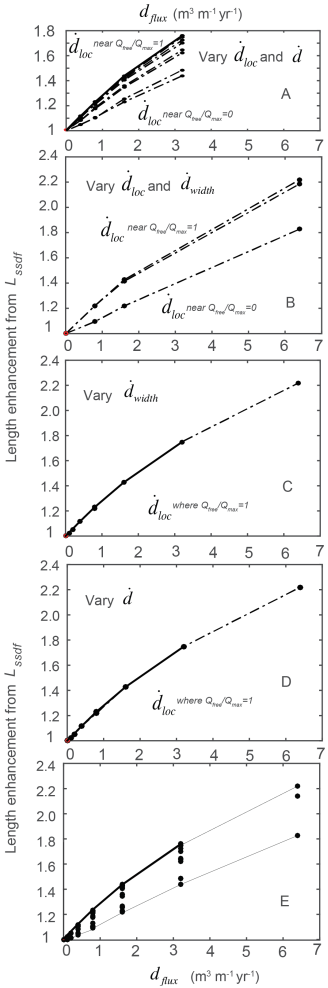

TCD
9, 6423–6470, 2015

Modeling debris-covered glaciers

L. S. Anderson and R. S. Anderson

Figure 9. Steady state length changes due to variations in debris delivery to the glacier. Glacier lengths are normalized by L_{ssdf}. The bold lines **(a, c–e)** connect results with the same parameters: $\dot{d}_{loc}$ and $\dot{d}_{width}$ are fixed at 42 % and 400 m. **(a)** Steady state glacier length from 36 simulations in which $\dot{d}$ and $\dot{d}_{loc}$ are varied with $\dot{d}_{width}$ fixed at 400 m. The multiple-dashed lines show the effect of changing $\dot{d}_{loc}$. The same results are presented in Fig. 7. **(b)** Steady state glacier length from simulations where $\dot{d}_{width}$ and $\dot{d}_{loc}$ are varied with $\dot{d}$ fixed at 8 mm yr^{-1}. **(c)** Length changes with $\dot{d}_{loc}$ fixed at 42 % while $\dot{d}_{width}$ is varied. **(d)** Length changes with $\dot{d}_{loc}$ fixed at 42 % while $\dot{d}$ is varied and $\dot{d}_{width}$ is constant. **(e)** Steady state glacier length from 72 simulations in which, $\dot{d}_{width}$, $\dot{d}$, and $\dot{d}_{loc}$ are varied.

TCD
9, 6423–6470, 2015

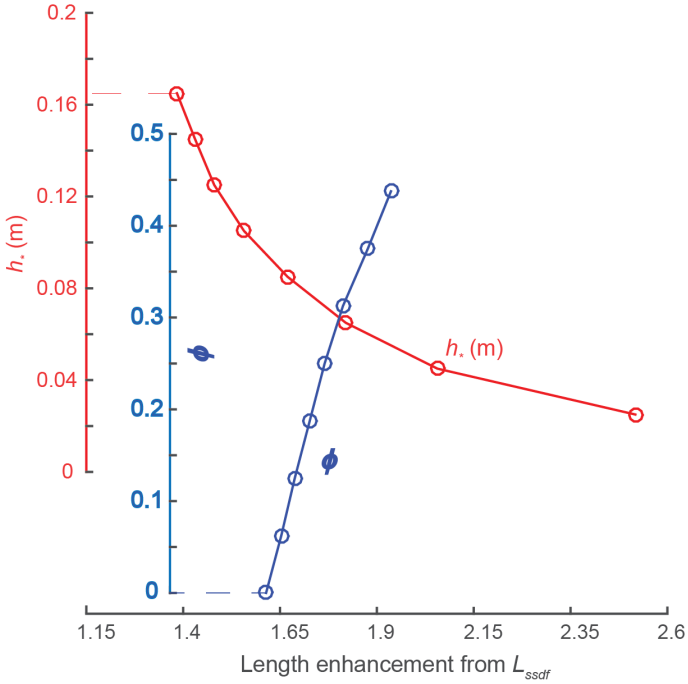

Figure 10. Sensitivity of steady state debris-covered glacier length to choices of h_* and ϕ. The lines intersect at the base parameter set. Parameter ranges are extreme to highlight the possible range of effects of each parameter.

TCD
9, 6423–6470, 2015

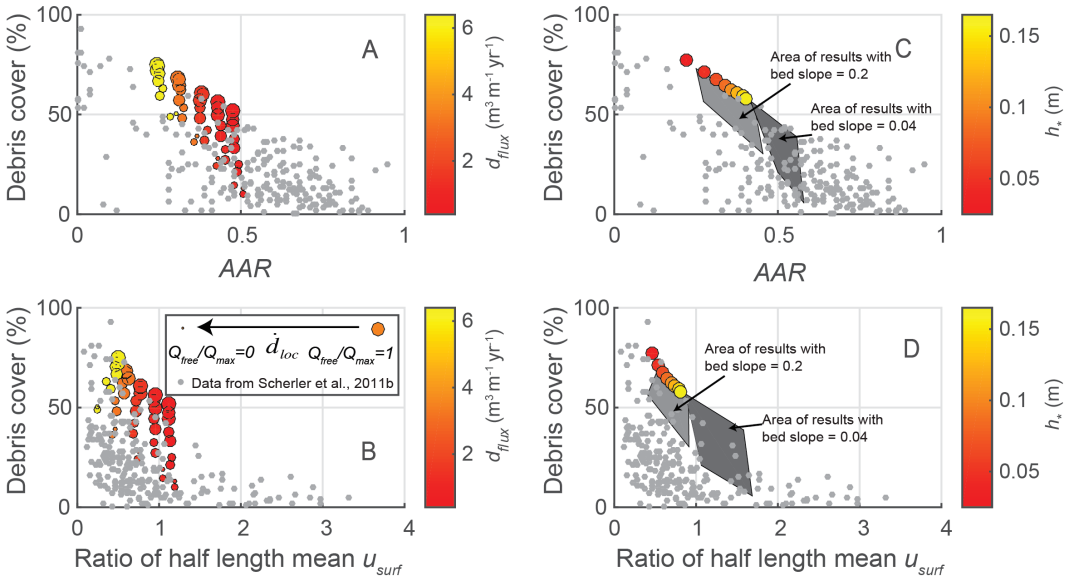

Figure 11. Comparison of steady state debris-covered model output with data from 287 glaciers in High Asia (Scherler et al., 2011b). **(a)** The AAR compared to debris cover percentage, d_{flux}, and $\dot{d}_{\text{loc}}$. **(b)** The ratio of the average surface speed of the lower 50 % of the glacier and the average surface speed of the upper 50 % of the glacier vs. debris cover percentage, d_{flux}, and $\dot{d}_{\text{loc}}$. **(c, d)** Same data as **(a, b)**, but exploring the effect of changing the bed slope and h_*. The quadrangles show the area occupied by simulation results using the same variables and parameters from **(a, b)** but with lower and higher bed slopes. h_* results are from the parameter test where h_* is varied, $\dot{d}_{\text{loc}}$ is 42 % and d_{flux} is 3.2 $\text{m}^3\,\text{m}^{-1}\,\text{yr}^{-1}$ (Fig. 10).

TCD
9, 6423–6470, 2015

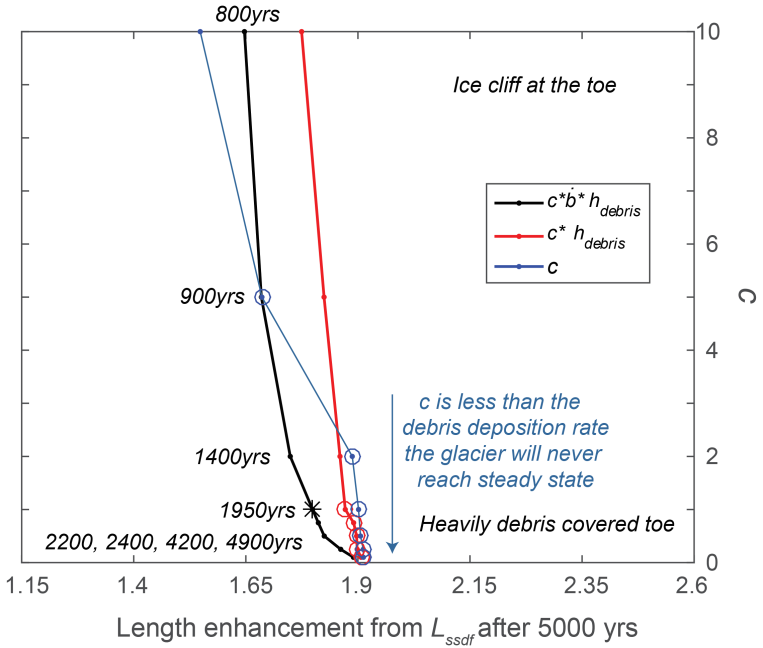

Figure 12. Exploring various choices for the $d_{\text{flux}}^{\text{snout}}$ parameterization. Glacier lengths are normalized by L_{ssdf}. Irrespective of the choice of the $d_{\text{flux}}^{\text{snout}}$ parameterization the steady glacier length is nearly doubled. Circles represent simulations in which M_{surface} (the total debris mass on the glacier) and glacier length did not reach steady state after 5000 years. For all simulations d_{flux} 3.2 $\text{m}^3\,\text{m}^{-1}\,\text{yr}^{-1}$. All simulations presented outside of this plot use the $d_{\text{flux}}^{\text{snout}} = c\dot{b}h_{\text{debris}}$ parameterization with $c = 1$ (* in the figure).

TCD
9, 6423–6470, 2015